



# USE OF HEAT EXCHANGER FOR PASSIVE CONTROL OF COMBUSTION INSTABILITIES

Aswathy Surendran and Maria A. Heckl

*School of Computing and Mathematics, Keele University, Staffordshire, ST5 5BG, United Kingdom*

*email: a.surendran@keele.ac.uk*

Naseh Hosseini

*Department of Mechanical Engineering, Eindhoven University of Technology, 5600 MB Eindhoven, The Netherlands*

O. J. Teerling

*Bekaert Combustion Technology BV, 9403 AR Assen, The Netherlands*

One of the major concerns in the operability of power generation systems is their susceptibility to combustion instabilities. In this work, we aim to examine the effective use of heat exchangers, an integral component in any power generation system, to passively control combustion instability. The combustor is modelled as a quarter-wave resonator (1-D, open at one end, closed at the other) with a compact heat source within, which follows time lag law for heat release. The heat exchanger (hex) is modelled as an array of tubes with bias flow and is placed near the closed end of the resonator, causing it to behave like a cavity-backed slit plate: an effective acoustic absorber. For simplicity and ease of analysis, we treat the physical processes of heat transfer and acoustic scattering occurring at the hex as two individual processes separated by an infinitesimal distance. The aeroacoustic response of the tube array is modelled using a quasi-steady approach and the heat transfer across the hex is modelled by assuming it to be a heat sink. Unsteady numerical simulations were carried out to obtain the heat exchanger transfer function (HTF), which is the response of the heat transfer at hex to upstream velocity perturbations. Combining the aeroacoustic response and the HTF, in the limit of the infinitesimal distance between these processes tending to zero, gives the net influence of the hex. Other parameters of interest are the heat source location and the cavity length (the distance between the tube array and the closed end). We then construct stability maps for the first resonant mode of the aforementioned combustor configuration, for various parameter combinations. Preliminary observations show that stability can be achieved for a wide range of parameters.

---

## 1. Introduction

Combustion systems are often affected by thermo-acoustic instabilities caused by a positive feedback between the acoustic pressure fluctuations and the unsteady heat release rate. In this study, we aim to investigate the effective use of heat exchangers to passively control the thermo-acoustic instability, by tuning the downstream acoustic properties of the combustion system. Our combustor is modelled as a quarter-wave resonator with a compact heat source. The heat exchanger (hex) is located near the closed end (downstream) of the resonator, causing it to behave like a cavity-backed tube row. The influence of hex on the stability of the combustor is examined through its aeroacoustic response to the incoming acoustic fluctuations as well as its heat transfer response to the upstream velocity fluctuations. These two physical processes are modelled and treated as individual processes,

separated by an infinitesimal distance. The aeroacoustic response of the hex tube row is modelled using the quasi-steady approach [1, 2] and the heat transfer response is obtained semi-empirically, using numerical simulations in ANSYS Fluent [3, 4] and curve-fitting approximations. The numerical simulations enable us to obtain a realistic heat transfer response of the hex.

## 2. Description of the system

The investigated combustion system consists of a quarter-wave resonator with both heat source (flame) as well as heat sink (hex) as shown in Fig. 1. The upstream end,  $x = 0$ , is open and the corresponding reflection coefficient is given by  $R_0 = -1$ . The heat source is located at a distance  $l_f$  from the upstream end and the hex is located at  $x = L$ . There are two processes occurring at the hex: the heat transfer at  $x = l_s$  and the acoustic reflection and transmission of incoming acoustic waves at  $x = L$ . For ease of analysis, we treat these processes as individual processes separated by an infinitesimal distance,  $\Delta x = L - l_s$ . The distance between the hex tube row and the closed downstream end of the resonator, referred to as cavity length, is denoted by  $l_c$ . The effective reflection coefficient of the hex (including heat transfer) backed by this cavity (shaded area in Fig. 1) is denoted as  $R_{eff}$ , which is derived in the subsequent sections.

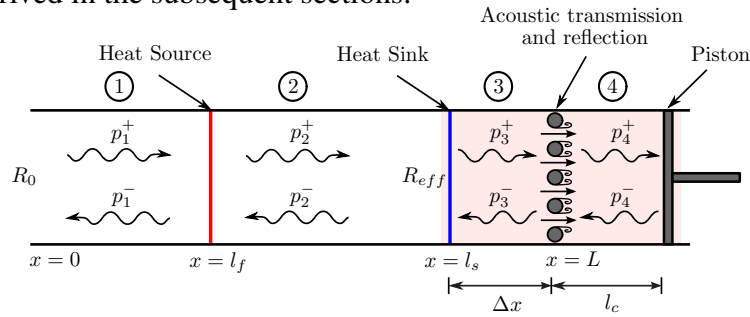


Figure 1: Schematic of the combustion system showing the incoming and reflected acoustic waves and those locations where different phenomena are assumed to occur.

### 2.1 Acoustic field

The acoustic waves are assumed to be one-dimensional and propagating perpendicular to the rods (normal incidence). The speed of sound and the temperature are assumed to be uniform throughout the resonator. The acoustic pressure and velocity fields within the combustor are denoted as

$$p_r(x) = p_r^+ + p_r^- = A_r e^{ik(x-l_f)} + B_r e^{-ik(x-l_f)}, \quad (1)$$

$$u_r(x) = u_r^+ + u_r^- = \frac{1}{\rho_0 c_0} \{p_r^+ - p_r^-\}, \quad (2)$$

where  $p^+$  and  $p^-$  are the forward and backward travelling pressure waves respectively,  $A$  and  $B$  are the pressure amplitudes and  $u^+$  and  $u^-$  are the acoustic velocities corresponding to  $p^+$  and  $p^-$  respectively. The subscript 'r' denotes the region within the combustor,  $\omega$  is the frequency of the acoustic wave,  $c_0$  is the speed of sound inside the resonator,  $k = \omega/c_0$  is the wavenumber and  $\rho_0$  is the density of the medium within the resonator. The factor  $e^{-i\omega t}$  is omitted throughout the analysis.

## 3. Model for the heat source

The heat source is assumed to be compact, planar and confined to an infinitesimally thin region at  $x = l_f$ . The heat release rate ( $\hat{Q}_f$ ) is assumed to follow the time-lag law, and to depend on the velocity fluctuations at the location,  $l_f$ , with a time-lag  $\tau$  and an interaction index  $n$  i.e.,

$$\hat{Q}_f(x, \omega) = n u_1(x) e^{i\omega\tau} \delta(x - l_f). \quad (3)$$

With Eq. (2),  $\hat{Q}_f(x, \omega)$  can be expressed in terms of the pressure

$$\hat{Q}_f(x, \omega)|_{x=l_f} = n e^{i\omega\tau} \frac{(p_1^+ - p_1^-)}{\rho_0 c_0}. \quad (4)$$

Across the heat source, at  $x = l_f$ , we assume continuity of pressure,

$$p_1^+ + p_1^- = p_2^+ + p_2^-, \quad (5)$$

and a velocity jump generated by the heat source [5],

$$(u_2^+ + u_2^-) - (u_1^+ + u_1^-) = \frac{(\gamma - 1)}{S \rho_0 c_0^2} \hat{Q}_f, \quad (6)$$

where  $S$  is the cross-sectional area of the duct and  $\gamma$  is the ratio of the specific heat capacities.

#### 4. Model of the heat sink

In this analysis, the hex is treated as a heat sink. The transient heat transfer response of the hex to the incoming velocity fluctuations is obtained using the transfer function approach [3] and a semi-empirical model is derived for the response using constrained least squares method. Numerical simulations were conducted using the transient CFD solver, ANSYS Fluent 15.0. A 2-D, laminar, incompressible flow was assumed in the domain. Rather than modelling the array of tubes, the computational domain was limited to half of the tube and half of the gap between the tubes, with symmetric boundary conditions on either side. At the inlet and outlet, ‘velocity inlet’ and ‘pressure outlet’ boundary conditions were imposed, respectively (Fig. 2).

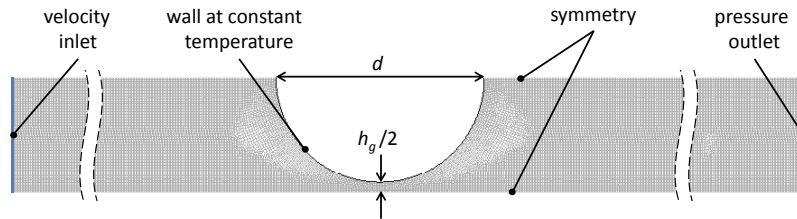


Figure 2: Meshed geometry with boundary conditions.

Across the heat sink, at  $x = l_s$ , we assume both pressure continuity,

$$p_2^+ + p_2^- = p_3^+ + p_3^-, \quad (7)$$

and velocity jump generated by the heat sink,

$$(u_3^+ + u_3^-) - (u_2^+ + u_2^-) = \frac{(\gamma - 1)}{S \rho_0 c_0^2} \hat{Q}_h, \quad (8)$$

where  $\hat{Q}_h$  is the heat transfer rate at hex, which will be calculated in subsequent sections.

##### 4.1 Numerical results for the $\hat{Q} - u$ relationship

In order to apply the transfer function approach, a ‘step’ perturbation was introduced at the inlet. The total velocity after the step perturbation will be  $U(t) = U_0 + u$ , where  $U_0$  is the mean inlet velocity before the step and  $u$  is the magnitude of the step perturbation at the inlet. An increment of  $u = 5\%$  of  $U_0$  was chosen to avoid any nonlinearities inherent in the system. The heat transfer at hex will then be:  $Q(t) = Q_{h,0} + Q_h$ , where  $Q_{h,0}$  is the mean heat transfer at the hex before the step and  $Q_h$  is the change in the heat transfer due to the velocity change. The transient simulations give the time response of the hex, which is then converted to the frequency response by fast Fourier transformation i.e.,  $u(t) \xrightarrow{FT} \hat{u}(\omega)$  and  $Q_h(t) \xrightarrow{FT} \hat{Q}_h(\omega)$ .

The heat exchanger transfer function (HTF), which is defined as

$$\text{HTF} = \frac{\hat{Q}_h/Q_{h,0}}{\hat{u}/U_0}, \quad (9)$$

is then calculated. Given the HTF, we can now deduce the  $\hat{Q} - u$  relationship from Eq. (9). HTF is a complex quantity with both magnitude,  $|\text{HTF}|$ , and phase,  $\Phi(\text{HTF})$ , and they depend on the flow field, geometry and frequency of the incoming perturbation. Hence, it is necessary to empirically obtain the expressions for HTF. Figures 3 (a) and (c) show the  $|\text{HTF}|$  and  $\Phi(\text{HTF})$  variations obtained for  $d = 3\text{mm}$  and  $h_g = 0.3\text{mm}$ , for incoming velocities  $U_0 = 0.1, 0.2$  and  $0.5$  m/s.

## 4.2 Analytical approximation for the $\hat{Q} - u$ relationship

The empirical expressions for HTF were obtained by assuming the following trial solutions for its magnitude and phase,

$$\log(|\text{HTF}|) = \begin{cases} a_0 + a_1f + a_2f^2 & f \leq f_p \\ b_0 + b_1\sqrt{f} & f \geq f_p \end{cases} \quad (10)$$

$$\Phi(\text{HTF}) = \begin{cases} e_0 + e_1f + e_2f^2 + e_3f^3 + e_4f^4 & f \leq f_p \\ g_0 + g_1\sqrt{f} + g_2f + g_3(\sqrt{f})^3 + g_4f^2 & f \geq f_p \end{cases} \quad (11)$$

$a_m, b_m, e_m$  and  $g_m$  are coefficients which are determined by a constrained least squares method [6]. Constraints are imposed at the first frequency value ( $f_0$ ) as well as an intermediate frequency ( $f_p$ ). Figures 3 (b) and (d) show the approximated  $|\text{HTF}|$  and  $\Phi(\text{HTF})$  for incoming velocities  $U_0 = 0.1, 0.2$  and  $0.5\text{m/s}$ . Here,  $f_p$  is 500Hz for the magnitude approximation of HTF and 200Hz for the phase approximation of HTF.

Substituting Eqs. (10) and (11) into Eq. (9) and taking  $\hat{u}$  to be the acoustic velocity fluctuation at  $x = l_s$ , we obtain,

$$\hat{Q}_h = (u_2^+ + u_2^-) (Q_{h,0}/U_0) \{|\text{HTF}| e^{i\Phi(\text{HTF})}\} \quad (12)$$

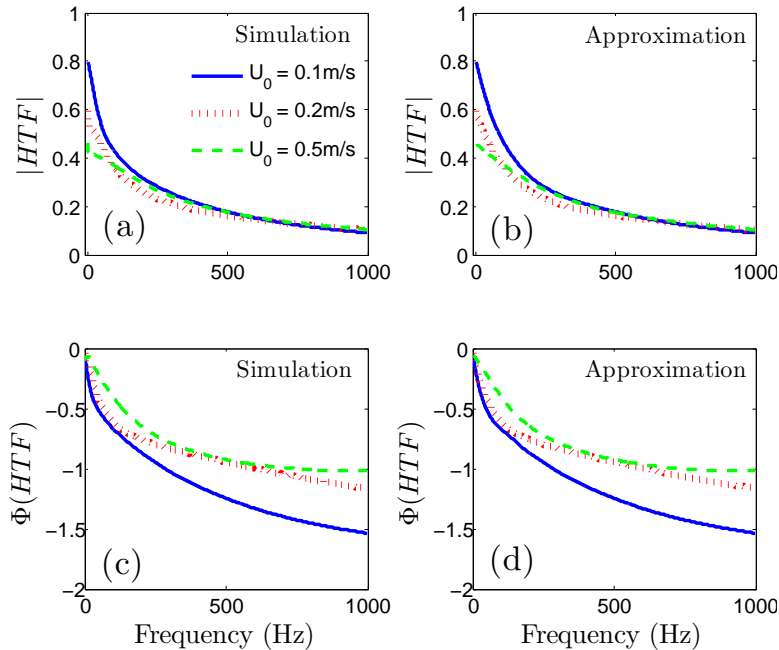


Figure 3: Comparison of  $|\text{HTF}|$  and  $\Phi(\text{HTF})$  obtained from numerical simulations ((a) and (c)) with their approximations ((b) and (d)), for  $d = 3\text{mm}$ ,  $h_g = 0.3\text{mm}$  and different velocities,  $U_0$ .

## 5. Model for the acoustic transmission and reflection coefficients of the hex

The tube row geometry is approximated to that of a duct with two half cylinders separated by a gap height of  $h_g$  (Fig. 4). Due to low Mach number, the flow within the approximated geometry is assumed to be incompressible and inviscid, except near the walls of hex tube where the viscous effects are confined to the boundary layer. Using conservation of mass (continuity) and momentum equations across different regions, one can derive the expressions for the transmission ( $T_h^\pm$ ) and reflection ( $R_h^\pm$ ) coefficients [1] as,

$$T_h^\pm = \frac{2}{2 + M_3 (S_p/S_j - 1)^2}, \quad (13)$$

$$R_h^\pm = \frac{M_3 (S_p/S_j - 1)^2}{2 + M_3 (S_p/S_j - 1)^2}, \quad (14)$$

where  $M_3 = U_0/c_0$  is the Mach number upstream of the tube row,  $U_0$  is the incoming flow speed,  $c_0$  is the speed of sound,  $S$  is the cross-sectional area of the duct and the subscripts 'p' and 'j' denote the duct and jet properties respectively. The assumption of incompressibility holds only in those cases where the jet Mach number ( $M_j$ ) is much smaller than 1. As  $M_j$  approaches 1, compressibility effects must be accounted for. Surendran et. al. [2] have derived and experimentally validated the expressions for the acoustic transmission and reflection coefficients of the geometry given in Fig. 4, in the case of compressible flow.

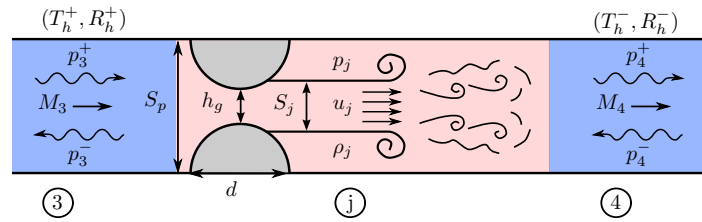


Figure 4: Schematic of the flow within the domain.

## 6. Model for the combined elements near the downstream end

The effective reflection coefficient  $R_{eff}$ , is the combined reflection coefficient of the backing plate, the hex located at a distance  $l_c$  in front of the plate and also the heat transfer process taking place at the hex (Fig. 1). In this analysis we assume the heat transfer process, given by Eq. (12), to happen at an infinitesimal distance  $\Delta x = L - l_s$  upstream of the actual hex geometry. The following conditions along with Eqs. (7) and (8) are used to obtain the effective reflection coefficient ( $R_{eff}$ ) of the cavity-backed hex with heat transfer.

At  $x = L + l_c$ ,

$$p_4^- = p_4^+ \quad (\text{complete reflection at the wall}). \quad (15)$$

At  $x = L$ , using Eqs. (13) and (14),

$$p_4^+ = T_h^+ p_3^+ + R_h^- p_4^-, \quad (16)$$

$$p_3^- = R_h^+ p_3^+ + T_h^- p_4^-. \quad (17)$$

Combining Eqs. (7) and (8) with Eqs. (15 - 17), we get the effective reflection coefficient as

$$R_{eff} = \frac{(p_2^-)}{(p_2^+)} = \frac{\alpha + (2 + \alpha) R e^{2ik\Delta x}}{(2 + \alpha) + \alpha R e^{2ik\Delta x}}, \quad (18)$$

where  $\alpha = ((\gamma - 1) (Q_{h,0}/U_0) \{|\text{HTF}| e^{i\Phi(\text{HTF})}\}) / (S\rho_0 c_0^2)$ , includes the effect of the heat transfer occurring at hex and

$$R = R_h^+ + \frac{T_h^+ T_h^- e^{2ikl_c}}{1 - R_h^- e^{2ikl_c}} \quad (19)$$

includes the effect of the geometry of the hex as well as the cavity [7].

In the limit of  $\Delta x \rightarrow 0$ , we get

$$R_{eff} = \frac{\alpha + (2 + \alpha)R}{(2 + \alpha) + \alpha R}. \quad (20)$$

## 7. Stability maps for the complete system

The combustion system shown in Fig. 1 can now be reduced to that of a duct, open at one end ( $x = 0$ ) and having a reflection coefficient of  $R_{eff}$  at the other end ( $x = L$ ). The heat source is located at  $x = l_f$ . The stability of the combustor is determined using the eigenvalue method [8] and the following conditions are used along with Eqs. (5) and (6) to form the characteristic equation of the system.

At  $x = 0$ ,

$$p_1^+ = R_0 p_1^- \quad (21)$$

At  $x = L$ ,

$$p_2^- = R_{eff} p_2^+ \quad (22)$$

where  $R_0$  and  $R_{eff}$  are the reflection coefficients at  $x = 0$  and  $x = L$  respectively.

Equations (5 - 6) and (21 - 22) are written as a matrix equation

$$[Y(\Omega)] \begin{bmatrix} p_1^+ \\ p_1^- \\ p_2^+ \\ p_2^- \end{bmatrix} = \begin{bmatrix} 0 \\ 0 \\ 0 \\ 0 \end{bmatrix}, \quad (23)$$

with matrix

$$[Y(\Omega)] = \begin{bmatrix} e^{-i\frac{\Omega}{c_0}l_f} & -R_0 e^{i\frac{\Omega}{c_0}l_f} & 0 & 0 \\ 0 & 0 & R_{eff} e^{i\frac{\Omega}{c_0}(L-l_f)} & e^{-i\frac{\Omega}{c_0}(L-l_f)} \\ 1 & 1 & -1 & -1 \\ -(1 + \beta e^{i\Omega\tau}) & (1 + \beta e^{i\Omega\tau}) & 1 & -1 \end{bmatrix}, \quad (24)$$

where  $\beta = (n(\gamma - 1)) / (S\rho_0 c_0^2)$ . The characteristic equation,  $\det Y(\Omega) = 0$ , is solved numerically by Newton-Raphson method or bisection method. The solution,  $\Omega$ , is a complex quantity of the form  $\Omega_m = \omega_m + i\delta_m$ , whose real part,  $\omega_m$ , gives the natural frequency of the mode  $m$ , and the imaginary part,  $\delta_m$ , gives the growth rate. The stability of the mode is determined from the sign of  $\delta_m$ . Positive  $\delta_m$  indicates instability and negative  $\delta_m$  indicates stability.

### 7.1 Properties of the system

*Fluid properties :*

$$c_o = 340 \text{ m/s}$$

(speed of sound)

$$\rho_o = 1.2 \text{ kg/m}^3$$

(density of medium)

$$\gamma = 1.4$$

(ratio of specific heat capacities)

*Duct properties :*

$$S = 0.05 \times 0.05 \text{ m}^2$$

(cross-sectional area of the duct)

$$L = 1 \text{ m}$$

(length of the duct)

*Heat release rate model :*

$$\tau = 0.15 \times 10^{-3} \text{ s}$$

(time-lag)

$$n = 187 \text{ kg m/s}^2$$

(interaction index)

$$\text{Heat source location : } l_f \in [0, L]$$

$$\text{Cavity length : } l_c \in [0, L/2]$$

## 7.2 Stability Maps

In this analysis, we are interested in the influence of the velocity of the flow incident on the hex ( $U_0$ ), the cavity-length ( $l_c$ ) and the heat source location ( $l_f$ ). The stability maps are constructed in the  $l_c - l_f$  plane. The *dark* regions indicate instability and the *white* regions indicate stability. Stability of the first mode of the system is determined from the sign of the growth rate,  $\delta_1$ , as aforementioned. Firstly, we construct the stability map for the combustion system without the heat exchanger tube row. In the absence of the hex,  $l_c$  is the extension to the duct length,  $L$ . The total length of the combustor will now be  $L + l_c$ . As expected, the resonator is always unstable (Fig. 5), regardless of the depth of the cavity or the location of the heat source.

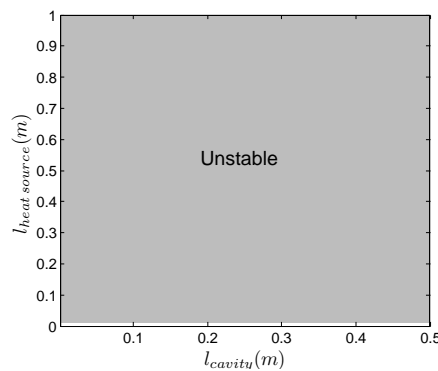


Figure 5: Stability map without hex and bias flow.

Next, we introduce the heat exchanger into the system. Figures 6 (a)-(c) show the stability maps obtained for different flow velocities. We observe that the region of stability increases as the velocity increases. Moreover, we can use a smaller cavity to stabilise the combustor, if we choose the flow velocity appropriately.

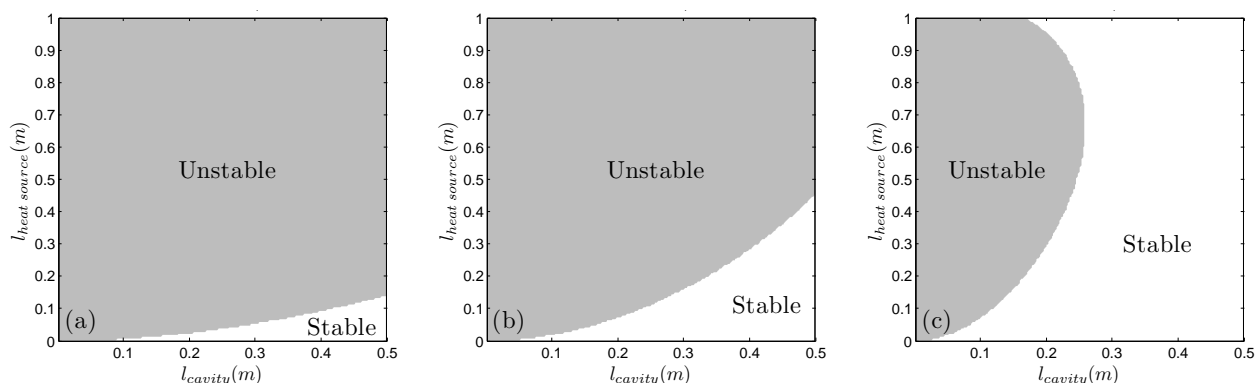


Figure 6: Stability maps for  $d = 3\text{mm}$ ,  $h_g = 0.3\text{mm}$  and (a)  $U_0 = 0.1\text{m/s}$ , (b)  $U_0 = 0.2\text{m/s}$  and (c)  $U_0 = 0.5\text{m/s}$ .

## 8. Conclusion and outlook

Stability analysis was conducted on a quarter-wave resonator including a heat source and a heat sink near the downstream closed end. In this analysis, we have included both the acoustic response

and a realistic heat transfer response of hex tube row. We observed that the unstable mode of the combustor can be stabilised by appropriately choosing the incoming flow velocity and the cavity length. Presently, work is in progress to extend the analysis to more realistic heat exchangers, e.g. multiple rows or other cross-sections.

## Acknowledgement

The presented work is part of the Marie Curie Initial Training Network Thermo-acoustic and Aero-acoustic Nonlinearities in Green combustors with Orifice structures (TANGO). We gratefully acknowledge the financial support from the European Commission under call FP7-PEOPLE-ITN-2012.

## REFERENCES

1. Hofmans, G. C. J., Boot, R. J. J., Durrieu, P. P. J. M., Auregan, Y. and Hirschberg, A., Aeroacoustics response of a slit-shaped diaphragm in a pipe at low Helmholtz number, 1: Quasi-steady results, *Journal of Sound and Vibration*, **244** (1), 35–56, (2001).
2. Surendran, A., Heckl, M. A., Boij, S., Bodén, H. and Hirschberg, A., Aeroacoustic response of an array of tubes with bias flow, *In Proceedings of the 23<sup>rd</sup> International Congress on Sound and Vibration*, Athens, Greece, (2016).
3. Hosseini, N., Kornilov, V., Teerling, O. J., Lopez Arteaga, I. and de Goey, L. P. H., Transfer function calculations of segregated elements in a simplified slit burner with heat exchanger, *In Proceedings of the 22<sup>nd</sup> International Congress on Sound and Vibration*, Florence, Italy, (2015).
4. Selimefendigil, F., Föller, S. and Polifke, W., Nonlinear identification of unsteady heat transfer of a cylinder in pulsating cross flow, *Computers & Fluids*, **53** (1), 1–14, (2012).
5. Heckl, M. A., Active control of the noise from a Rijke tube, *Journal of Sound and Vibration*, **124** (1), 117–133, (1988).
6. Lawson, C. L. and Hanson, R. J., *Solving Least Squares Problems*, The Society for Industrial and Applied Mathematics, (1995).
7. Surendran, A. and Heckl, M. A., Analytical study of a Rijke tube with heat exchanger, *In Proceedings of the 21<sup>st</sup> International Congress on Sound and Vibration*, Beijing, China, (2014).
8. Heckl, M. A., *Heat Sources in Acoustic Resonators*, University of Cambridge, PhD Thesis, (1985).